frontiers | Frontiers in Immunology

TYPE Original Research
PUBLISHED 06 December 2024
DOI 10.3389/fimmu.2024.1483617

OPEN ACCESS

EDITED BY
Penny Fang,
University of Texas MD Anderson Cancer Center, United States

REVIEWED BY
Eden Kleiman,
JSR Life Sciences, United States
Zhenyu Dai,
Stanford University, United States

*CORRESPONDENCE
Sandra Kleinau
sandra.kleinau@icm.uu.se

RECEIVED 20 August 2024
ACCEPTED 14 November 2024
PUBLISHED 06 December 2024

CITATION
Nguyen OTP, Lara S, Ferro G, Peipp M and Kleinau S (2024) Rituximab-IgG2 is a phagocytic enhancer in antibody-based immunotherapy of B-cell lymphoma by altering CD47 expression.
Front. Immunol. 15:1483617.
doi: 10.3389/fimmu.2024.1483617

Rituximab-IgG2 is a phagocytic enhancer in antibody-based immunotherapy of B-cell lymphoma by altering CD47 expression

Oanh T. P. Nguyen[1], Sandra Lara[1], Giovanni Ferro[1], Matthias Peipp[2] and Sandra Kleinau[1]*

[1]Department of Cell and Molecular Biology, Uppsala University, Uppsala, Sweden, [2]Division of Antibody-Based Immunotherapy, University Hospital Schleswig-Holstein, Kiel, Germany

Antibody-dependent cellular phagocytosis (ADCP) by monocytes and macrophages contributes significantly to the efficacy of many therapeutic monoclonal antibodies (mAbs), including anti-CD20 rituximab (RTX) targeting $CD20^+$ B-cell non-Hodgkin lymphomas (NHL). However, ADCP is constrained by various immune checkpoints, notably the anti-phagocytic CD47 molecule, necessitating strategies to overcome this resistance. We have previously shown that the IgG2 isotype of RTX induces CD20-mediated apoptosis in B-cell lymphoma cells and, when combined with RTX-IgG1 or RTX-IgG3 mAbs, can significantly enhance Fc receptor-mediated phagocytosis. Here, we report that the apoptotic effect of RTX-IgG2 on lymphoma cells contributes to changes in the tumor cell's CD47 profile by reducing its overall expression and altering its surface distribution. Furthermore, when RTX-IgG2 is combined with other lymphoma-targeting mAbs, such as anti-CD59 or anti-PD-L1, it significantly enhances the ADCP of lymphoma cells compared to single mAb treatment. In summary, RTX-IgG2 acts as a potent phagocytic enhancer by promoting Fc-receptor mediated phagocytosis through apoptosis and reduction of CD47 in $CD20^+$ malignant B-cells. RTX-IgG2 represents a valuable therapeutic component in enhancing the effectiveness of different mAbs targeting B-cell NHL.

KEYWORDS

anti-CD20 antibody, apoptosis, CD47, cancer immunotherapy, monocyte, phagocytosis, rituximab

1 Introduction

Among various hematological malignancies classified under non-Hodgkin lymphoma (NHL), B-cell lymphoma is the most prevalent subtype (1). In the past decades, the survival rate of B-cell lymphoma patients has been significantly improved thanks to advancements in therapeutic monoclonal antibodies (mAbs). Nevertheless, predicting the treatment responses of most B-cell lymphomas remains challenging due to their significant heterogeneity, highlighting the critical need for ongoing research to improve treatment efficacy and address these complexities (2).

Since its initial approval in 1997, the chimeric CD20-targeting IgG1 mAb rituximab (RTX) has remained a cornerstone in cancer immunotherapy (3). Despite its widespread use, the precise *in vivo* mechanisms of RTX's action remain uncertain (4). Preclinical and clinical data have associated RTX's efficacy in eliminating $CD20^+$ lymphoma cells with various immune responses such as antibody-dependent cellular phagocytosis (ADCP), complement-dependent cytotoxicity (CDC), and to a lesser extent, apoptosis (5–7). Increasing evidence now suggests that the efficacy of RTX monotherapy is primarily mediated through Fc receptor (FcR)-dependent phagocytosis by monocytes and macrophages (6, 8–13). However, opsonization with RTX alone often fails to induce a complete eradication of the target cells, indicating the presence of resistance mechanisms (3).

In recent years, a number of important insights into the regulation of phagocytosis have been established. CD47, a transmembrane protein, has been identified as a crucial regulator of phagocytosis by providing an anti-phagocytic (or "don't-eat-me") signal (14). CD47 achieves its anti-phagocytic effect by binding to its cognate receptor – the signal regulatory protein-α (SIRP-α) – which is highly expressed on macrophages (15, 16). CD47 is ubiquitously expressed in the body and acts as a "marker-of-self", protecting healthy cells from being phagocytosed, thus maintaining immune homeostasis and preventing autoimmunity (15). Senescent or damaged cells, for example, erythrocytes, and apoptotic cells have been shown to have reduced CD47 expression or express CD47 with altered conformation. These alterations consequently render the anti-phagocytic CD47/SIRP-α signal ineffective and allow for the removal of these cells (17–20). Interestingly, recent studies have shown that various malignancies overexpress CD47 as a part of their immune evasion, dampening ADCP induced by therapeutic mAbs (15, 16). This suggests that disrupting CD47-SIRP-α interaction may be pro-phagocytotic, thus potentially improving the therapeutic efficacy of anti-tumor mAbs. Indeed, Métayer et al. showed that blocking CD47 greatly increased phagocytosis of B-cell lymphoma cells by macrophages (21). Along the same lines, Chao et al. reported a synergistic ADCP-mediated anti-tumor activity when combining a CD47-blocking mAb with RTX (13). Despite these promising findings, clinical trials have revealed significant toxicity associated with CD47-blocking mAbs, including anemia, neutropenia, and thrombocytopenia (15, 22). Nonetheless, CD47 remains a potential therapeutic target for improving the efficacy of anti-tumor Abs, provided that the therapy of choice selectively targets only CD47 on the target tumor cells.

We have previously demonstrated that the IgG2 isotype of RTX (RTX-IgG2) is capable of inducing CD20-mediated apoptosis in B-cell lymphoma cells (9). When combining RTX-IgG2 with the phagocytosis-efficient RTX-IgG1 or RTX-IgG3, it significantly enhances phagocytosis of B-cell lymphoma cells. In contrast, a combination of RTX-IgG1 and RTX-IgG3 does not enhance ADCP of B-cell lymphoma cells (9). This suggests that RTX-IgG2 is specific in enhancing the efficacy of other RTX isotypes without contributing to adverse effects.

Here, we aim to investigate the mechanisms underlying the enhancing effect of RTX-IgG2 on phagocytosis when combined with other RTX isotypes and further explore its potential when combined with mAbs targeting other lymphoma antigens (CD59 and PD-L1). Our findings reveal, for the first time, that RTX-IgG2-mediated apoptosis is associated with a reduced and altered CD47 expression on $CD20^+$ B-cell lymphoma cells, enhancing FcR-mediated phagocytosis by tumor-specific mAbs.

2 Materials and methods

2.1 Cell cultures

The human acute monocytic leukemia cell line MonoMac-6, kindly provided by Dr. Helena Jernberg Wiklund (Department of Immunology, Genetics and Pathology (IGP), Uppsala University, Uppsala, Sweden) and authenticated by STR-profiling (Microsynth AG, Balgach, Switzerland), was used as monocytic effector cells in the ADCP assay. MonoMac-6 cells express the phagocytosis-regulating receptor FcγRII (CD32) (Supplementary Figure S1A) as well as FcγRI (CD64) (9) and display SIRP-α (Supplementary Figure S1B). MonoMac-6 cells were cultured in complete Roswell Park Memorial Institute medium (cRPMI) that contained RPMI 1640 (21875034, Thermo Fisher Scientific), 10% heat-inactivated (h.i.) fetal bovine serum (FBS) (11550356, Thermo Fisher Scientific), and 1% Penicillin-Streptomycin (PenStrep) (P4333, Merck, Darmstadt, Germany).

The CD20-expressing B-cell lymphoma cell lines Granta-519 and Raji – originating from human mantle cell lymphoma and Burkitt lymphoma, respectively – were used as tumor target cells. Granta-519 cell line was purchased from the German Collection of Microorganisms and Cell Culture (ACC 342, DMSZ, Braunschweig, Germany) and was cultured in Dulbecco's Modified Eagle Medium (DMEM) (11965092, Thermo Fisher Scientific, Waltham, MA, USA) with addition of 10% h.i. FBS and 1% PenStrep (complete DMEM; cDMEM). Raji cell line was kindly provided by Dr. Fredrik Öberg (IGP, Uppsala University), authenticated by STR-profiling at Microsynth AG, and cultured in cRPMI.

The human B-cell precursor leukemia cell line Reh, lacking expression of CD20 (Supplementary Figure S2A), was used as control cells. Reh cells were kindly provided by Dr. Ola Söderberg (Department of Pharmaceutical Biosciences, Uppsala University) and maintained in cRPMI.

All cells were cultured in suspension cell culture flasks (3910.502, Sarstedt, Nümbrecht, Germany) using a humidified cell culture incubator (InCuSafe, LabRum, Östersund, Sweden) at 37°C under 5% CO_2. The cells were routinely tested for mycoplasma contamination using MycoStrip™ detection kit (rep-mys, *In vivo*Gen, San Diego, CA, USA).

2.2 Antibodies

The human anti-CD20 (RTX) isotype family, including IgG1, IgG2, IgG3, and IgG4 anti-CD20 mAbs, was purchased from *In vivo*Gen (hcd20-mab1, hcd20-mab2, hcd20-mab3, and hcd20-mab4). Human recombinant isotype controls (kappa allotype) IgG1, IgG2, IgG3, and IgG4 were obtained from BioRad (Hercules, CA, USA) (HCA192, HCA193, HCA194, HCA195). Blocking of CD47 was performed with purified mouse anti-human CD47 mAb (αCD47-fuFc) clone CC2C6 (323102, Biolegend, San Diego, CA, USA) and humanized anti-CD47 IgG2σ mAb (αCD47-siFc) – a variant of magrolimab harboring a completely silenced Fc (23).

For cell surface staining, the following mAbs were used: APC-conjugated mouse IgG2a anti-human CD20 (clone LT20, H12155A, EuroBioScience, Friesoythe, Germany), PE-conjugated mouse IgG1 anti-human CD47 (clone CC2C6, 323108, Biolegend), PE-conjugated mouse IgG2a anti-human CD59 (clone p282 (H19), 304707, Biolegend), recombinant human IgG1 anti-human PD-L1 (hpdl1-mab1, *In vivo*Gen), APC-conjugated mouse anti-human IgG secondary Ab (αhIgG-APC) (562025, BD Biosciences, Franklin Lakes, NJ, USA), APC-conjugated mouse IgG2a anti-human SIRP-α Ab (clone 15-414, 372109, Biolegend), and FITC-conjugated mouse IgG2b anti-human CD32 Ab (clone IV.3, 60012Fl.1, StemCell Technologies, Vancouver, BC, Canada). Mouse isotype controls, including APC-conjugated IgG2a, PE-conjugated IgG1, PE-conjugated IgG2a, and FITC-conjugated IgG2b (C12386A, C12385B, C12386P, C12387F), were purchased from EuroBioScience.

2.3 Antibody-dependent cellular phagocytosis

MonoMac-6 effector cells were stained with 10 µM of CellTrace™ Far Red dye (CTFR, C34564, Thermo Fisher Scientific) in PBS (M09-9400-100, Medicago, Quebec City, QC, Canada), at 10^6 cells/mL for 20 min at 37°C. After washing with pre-warmed cRPMI (to remove excessive dye), the cells were adjusted to 7.5×10^5 cells/mL and stimulated with recombinant human interferon γ (IFNγ, PHP050, BioRad) at 0.2 µg/mL for 3 hours at 37°C. Meanwhile, Granta-519 target cells were stained with Vybrant™ CFDA SE dye (CFSE, V12883, Thermo Fisher Scientific) following manufacturer's instruction before seeding for monolayers at a cell density of 7.5×10^4 cells/100 µL per well in a round-bottomed 96-well plate (83.3925, Sarstedt). After 3 hours, MonoMac-6 cells were harvested, resuspended at 7.5×10^4 or 15×10^4 cells/100 µL per well (for an effector to target (E:T) ratio of 1:1 or 2:1, respectively), and added to the target cells for co-culturing. For the co-cultures, both cell types were resuspended in an assay medium ($cDMEM_{low\text{-}Glu}$) which contained low-glucose (1 g/L) DMEM (31885023, Thermo Fisher Scientific), 10% h.i. FBS, and 1% PenStrep. Co-cultures of effectors and target cells were immediately incubated with RTX or isotype control Abs at a concentration of 1.5 µg/mL, and kept at 37°C for 1 hour. Untreated co-cultures were used as negative controls. After 1 hour, the plate was centrifuged at 500 ×g for 3 min at 4°C and the supernatant was removed. Cells were washed twice with 250 µL of cold PBS containing 0.5% h.i. FBS (flow staining buffer). After the last washing step, cells were resuspended in 100-200 µL of cold flow staining buffer, kept on ice, and analyzed immediately using a MACSQuant VYB flow cytometer (Miltenyi Biotec, Bergisch Gladbach, Germany). Before analyzing cell samples, the flow cytometer was calibrated with MACSQuant Calibration Beads (130-093-607, Milteny Biotec) and compensation was performed using unstained and single-stained samples. A minimum of 15'000 events were acquired for each sample. $CTFR^+$ $CFSE^+$ MonoMac-6 cells were considered positive phagocytic cells.

For enhanced phagocytosis assays, target cells (7.5×10^4 cells/100 µL per well) were pre-incubated with RTX-IgG2 (1.5 µg/mL), αCD47-fuFc (1 µg/mL), or αCD47-siFc (10 µg/mL), for 30 min before addition of MonoMac-6 cells and RTX-IgG1 or RTX-IgG3 (1.5 µg/mL). In another set of experiments, the same amount of target cells per well was treated with staurosporine (STR, S1421, Selleck Chemicals, Houston, TX, USA) at 7.5 µM for 6 hours at 37°C prior to incubation with effector cells and RTX-IgG1 or RTX-IgG3 for 1 hour. Dimethyl sulfoxide (DMSO, D8418, Merck) was used to prepare the STR stock solution and thus, was used as vehicle control for these experiments.

2.4 Apoptosis assay and CD47 expression analysis

Granta-519 cells were seeded in monolayers at a cell density of 7.5×10^4 cells/100 µL per well in a round-bottomed 96-well plate prior to treatment. The cells were then incubated with 7.5 µM STR for 6 hours or 1.5 µg/mL of RTX isotypes for 30 min at 37°C. After centrifugation for 5 min at 600 ×g at 4°C, cells were washed with cold flow staining buffer, resuspended in 50 µL of flow staining buffer containing 1× LIVE/DEAD™ Fixable Violet dye (DC-Violet, L34963, Thermo Fisher Scientific) and 1× Human TruStain FcX™ (Fc Receptor Blocking Solution, 422302, Biolegend), and kept at room temperature (RT) for 10 min. Positive controls for DC-Violet were prepared by treating Granta-519 cells with 90% ethanol (20821.310, VWR, Radnor, PA, USA) for 1 min. Subsequently, PE-IgG1 anti-CD47 and PE-IgG1 isotype control Abs were added and the cells were stained for 30 min on ice. Cells were subsequently centrifuged at 600 ×g at 4°C, washed with flow staining buffer, resuspended in 100 µL of FITC-conjugated Annexin V (640906, Biolegend) prepared in 1× Annexin V binding buffer (556454, BD Biosciences), and stained for 15 min at RT. After adding 100 µL of 1× Annexin V binding buffer per well, cells were collected and analyzed using the MACSQuant VYB flow cytometer. Unstained and single-stained samples were used for compensation and gating.

A minimum of 10'000 events were acquired for each sample. DC-Violet$^+$ cells were considered necrotic cells and thus, excluded from further analyses. All DC-Violet$^-$ cells were analyzed for CD47 expression, and Annexin V$^+$ DC-Violet$^-$ Granta-519 cells were considered apoptotic cells.

2.5 Immunofluorescence staining and fluorescence microscopy

For live-cell imaging, Granta-519 and MonoMac-6 cells were prepared according to the ADCP protocol before being loaded into a flat-bottomed 96-well plate (32096, SPL Life Sciences Co., Ltd., Gyeonggi-do, Korea). Live-cell imaging was performed after 1 hour of incubation at 37°C on a fluorescence Nikon Eclipse Ti microscope (Nikon Europe B.V., Amsterdam, Netherlands) using a Plan Apo 10×/0.45 objective.

To analyze the expression of CD47, RTX- or STR-treated Granta-519 cells were washed with cold flow staining buffer and fixed with 50 µL of fixation buffer (88-8824, Thermo Fisher Scientific) for 15 min on ice. The fixed cells were washed twice with cold flow staining buffer and blocked by 1% bovine serum albumin (BSA, Fraction V, 422371X, VWR) in PBS for 1 hour. Next, the cells were incubated overnight at 4°C with 3 µg/mL of CF®640R-conjugated mouse anti-human CD47 Ab (clone B6H12.2, BNC400437-100, Biotium, Fremont, CA, USA) and 1× Hoechst 33342 Ready Flow™ Reagent (R37165, Thermo Fisher Scientific) prepared in 1% BSA in PBS. Stained cells were then washed, centrifuged, re-dispersed in 20 µL of deionized water, and added onto Superfrost plus microscope slides (J1800AMNZ, Thermo Fisher Scientific) for air-drying. Glass coverslips (#1.5, 12323148, Fisher Scientific, Hampton, NH, USA) were mounted on the microscope slides using Epredia™ Immu-Mount™ mounting medium (10662815, Fisher Scientific). Fluorescence images of mounted cells were acquired with a Zeiss LSM 700 confocal microscope (Carl Zeiss AG, Oberkochen, Germany) using a Plan-Apochromat 63×/1.4 Oil DIC M27 objective.

2.6 Data analysis

Microscope images were processed and analyzed by ZEISS ZEN lite (black edition) software (Carl Zeiss AG) or the open-source Java application ImageJ (https://imagej.nih.gov/ij/). Flow cytometry data were analyzed by FlowJo 10.9.0 software (BD Biosciences). Data were statistically analyzed with one-way ANOVA with Tukey-Kramer *post-hoc* test and visualized using GraphPad Prism 10.2.2 software (GraphPad Software, Boston, MA, USA). All results are displayed as mean ± standard error of the mean (SEM) of three independent experiments with a significance of $p<0.05$, unless indicated differently. All data were visualized by Adobe Illustrator (Adobe Inc., San Jose, CA, USA) using input files from the aforementioned software.

3 Results

3.1 ADCP induced by RTX-IgG1 or RTX-IgG3 is enhanced if combined with RTX-IgG2

The capacity of different anti-CD20 RTX isotype variants to stimulate human monocytes to phagocytose CD20$^+$ B-cell lymphoma cells varies significantly, and use of certain isotype combinations can further improve the ADCP function (9, 10). Indeed, *in vitro* ADCP analyses of human FcR-positive monocytic MonoMac-6 cells, in co-cultures with human CD20$^+$ B-cell lymphoma Granta-519 cells opsonized with different IgG isotypes of RTX, demonstrate that RTX-IgG3 is more effective than RTX-IgG1 in inducing phagocytosis (Figure 1A) (Supplementary Figures S3, S4). In contrast, RTX-IgG2 exhibits quite modest phagocytic activity (Figure 1A) (Supplementary Figure S3). However, when RTX-IgG2 is combined with either RTX-IgG1 or RTX-IgG3, it significantly enhances the ADCP response compared with RTX-IgG1 or RTX-IgG3 alone (Figures 1A, B).

As shown in Table 1, RTX-IgG1 achieves an approximately 19% increase in ADCP when combined with RTX-IgG2, while RTX-IgG3 shows an increase of about 12% when combined with RTX-IgG2. This phagocytosis-enhancing effect of RTX-IgG2 has been associated with CD20-mediated apoptosis, but the mechanisms involved remain unclear (9). To address this gap, we have delved deeper into the phagocytic enhancing effect by RTX-IgG2.

3.2 RTX-IgG2 induces significant CD20-mediated apoptosis but minor necrosis

To study the role of apoptosis in ADCP, we first optimized the concentration and treatment duration of RTX-IgG2 in relation with the apoptosis-inducing agent STR in Granta-519 cells, while minimizing necrosis. We identified that RTX-IgG2, at a concentration of 1.5 µg/mL, and STR at 7.5 µM, induced comparable levels of apoptosis (27% ± 1.7 and 26% ± 1.3, respectively), which were significantly higher than apoptosis levels observed in untreated Granta-519 cells (10% ± 1) (Figures 2A, B, Supplementary Figures S5A, D). In contrast, RTX-IgG1 and RTX-IgG3 did not induce apoptosis in the Granta-519 cells (Figures 2A, B). Notably, RTX-IgG2 was able to induce a comparable level of apoptosis as STR, but within a significantly shorter timeframe – 30 min for RTX-IgG2 versus 6 hours for STR. Moreover, RTX-IgG2-induced apoptosis was accompanied by negligible levels of necrosis compared to untreated controls (Figure 2C, Supplementary Figure S5B). Similarly, neither RTX-IgG1 nor RTX-IgG3 induced necrosis. STR induced approximately 20% more necrosis in Granta-519 cells compared to untreated controls (Figure 2C, Supplementary Figure S5E), yet the level of necrosis in STR-treated cells remained relatively low, accounting for less than 12% of the total analyzed cell population.

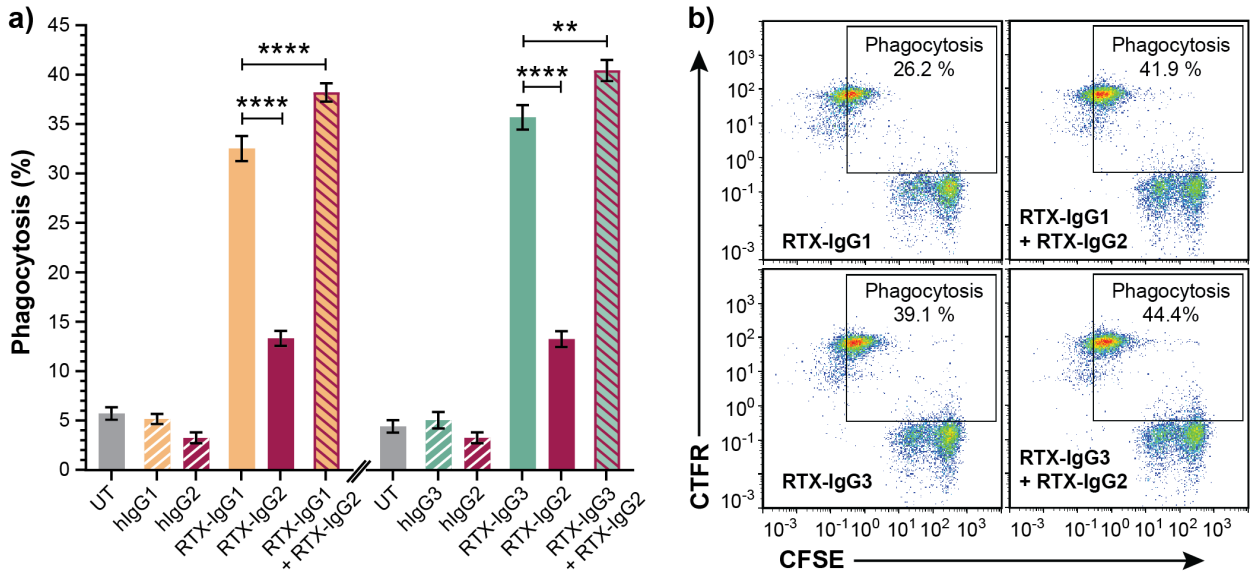

FIGURE 1
RTX-IgG2 enhances phagocytosis of RTX-IgG1- or RTX-IgG3-treated CD20$^+$ B-cell lymphoma cells. Flow cytometry analysis of ADCP of Granta-519 B-cell lymphoma cells, treated with anti-CD20 RTX isotypes or human isotype control Abs (1.5 µg/ml), by MonoMac-6 cells at an E:T ratio of 1:1. **(A)** Percentage phagocytosis of Granta-519 cells induced by single RTX isotypes, or dual combinations of RTX-IgG2 with RTX-IgG1 or RTX-IgG3. Untreated cells (UT), and human Ab isotypes: hIgG1, hIgG2, hIgG3, were used as controls. For dual treatments, Granta-519 cells were pre-opsonized with 1.5 µg/mL of RTX-IgG2 for 30 min followed by 1.5 µg/mL of RTX-IgG1 or RTX-IgG3. Results are shown as mean ± SEM of three independent experiments, each with three biological replicates. Statistical analysis by one-way ANOVA with Tukey-Kramer post-hoc test (****p<0.0001, **p<0.01). **(B)** Representative bivariate plots showing phagocytosis of RTX-treated CFSE-labeled Granta-519 target cells by CTFR-labeled MonoMac-6 effector cells. Phagocytosis was quantified as the percentage of double positive CFSE$^+$ CTFR$^+$ MonoMac-6 cells (square gate). Increased phagocytosis was observed when RTX-IgG2 was combined with RTX-IgG1 or RTX-IgG3.

TABLE 1 **Summary of percentage increase in phagocytosis of CD20$^+$ B-cell lymphoma cells (Granta-519) induced by tumor-specific mAb (anti-CD20 RTX, anti-CD59, or anti-PD-L1) in combination with RTX-IgG2 or anti-CD47 mAb (where applicable) in comparison with single use of tumor-specific mAb.**

Treatment	RTX-IgG1	RTX-IgG3	αCD59	αPD-L1
+RTX-IgG2	19%*	12%	44%	31%
+αCD47-fuFc	52%	28%	nd	nd
+αCD47-siFc	42%	17%	nd	nd

*Mean (%); fuFc, functional Fc domain; siFc, silenced Fc domain; nd, not determined.

Control experiments with a human CD20-negative B-cell precursor leukemia cell line (Reh) (24) further affirmed that the apoptosis induced by RTX-IgG2 was CD20-dependent as RTX-IgG2 did not induce apoptosis or necrosis in the Reh cells (Supplementary Figures S2B, C).

3.3 Apoptosis enhances FcR-mediated phagocytosis

To verify that apoptosis contributes to enhanced ADCP, we also investigated the effect of CD20-independent apoptosis, induced by STR, on ADCP mediated by RTX isotypes. Indeed, when combined with RTX-IgG1 or RTX-IgG3 treatment on Granta-519 cells, STR significantly enhanced ADCP compared to single RTX treatment (Figure 3). Unaccompanied use of STR resulted in higher ADCP of Granta-519 cells compared to untreated controls, although at inferior levels compared to anti-CD20 mAb single treatment (Figure 3).

3.4 Apoptosis enhances RTX-mediated phagocytosis by impairing "don't-eat-me" CD47 expression

The level of "don't-eat-me" anti-phagocytic CD47 protein varies on the surfaces of different B-cell lymphoma cell lines (Supplementary Figure S6A). Among the tested cell lines, Granta-519 cells expressed the highest level of CD47, implying its high resistance to ADCP (Supplementary Figure S6B). Interestingly, we discovered that apoptosis, induced by either RTX-IgG2 or STR, led to a reduction of CD47 expression in Granta-519 cells (Figures 4A, B). STR – being a very efficient apoptosis inducer – significantly reduced the expression level of CD47 to 0.55-fold of the level detected in untreated cells (Figure 4B) (Supplementary Figure S5F). Similarly, CD20-mediated apoptosis induced by RTX-IgG2 reduced the expression level of CD47 in Granta-519 cells to 0.78-fold of the level detected in untreated cells, corresponding to a 22% reduction in CD47 on the cell surface (Figure 4B, Supplementary Figure S5C).

The expression pattern of CD47 on the cell surface was further examined using confocal microscopy. As shown by Figure 4C (upper panel), CD47 was evenly distributed on the cell membrane of untreated and RTX-IgG1-treated Granta-519 cells. In contrast, RTX-IgG2- or STR-treated Granta-519 cells showed decreased

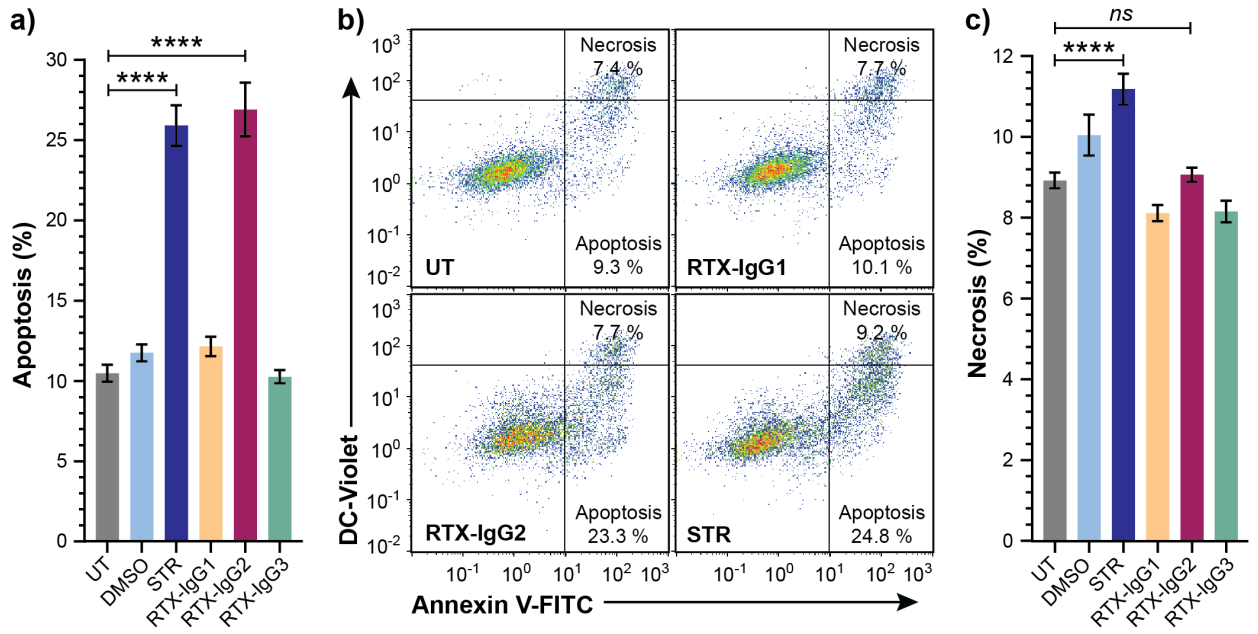

FIGURE 2
Analysis of cell death in CD20$^+$ B-cell lymphoma cells treated with STR or RTX isotypes. Granta-519 cells treated with STR (6 hours) or RTX isotypes (30 min) were analyzed for apoptosis or necrosis compared to untreated cells (UT). Dimethyl sulfoxide (DMSO) was used as vehicle control of STR treatment. **(A)** Percentage apoptosis in UT or treated Granta-519 cells. **(B)** Representative bivariate plots of Granta-519 cells, showing apoptosis and necrosis, in UT and after treatment with RTX isotypes or STR. Apoptotic cells were identified as Annexin V$^+$ DC-Violet$^-$ cells, while double positive (Annexin V$^+$ DC-Violet$^+$) cells were identified as necrotic cells with compromised cell membrane. **(C)** Percentage necrosis in UT or treated Granta-519 cells. Results in **(A, C)** show mean ± SEM of three independent experiments, each with three biological replicates. Statistical analysis by one-way ANOVA with Tukey-Kramer post-hoc test (****p<0.0001; ns, not significant).

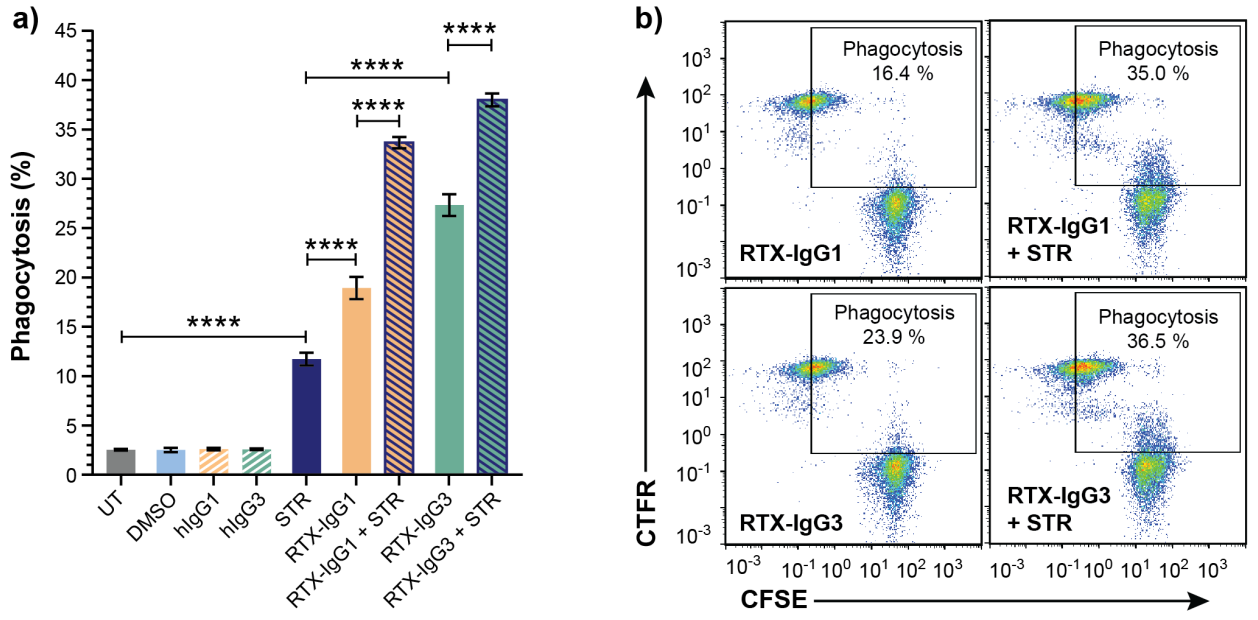

FIGURE 3
Apoptosis induced by STR in CD20$^+$ B-cell lymphoma cells enhances ADCP. Flow cytometry analysis of phagocytosis of Granta-519 cells, untreated (UT) or incubated with STR for 6 hours before addition of RTX isotypes or isotype controls (1.5 µg/mL), by MonoMac-6 cells (E:T ratio = 1:1). **(A)** Percentage phagocytosis of UT Granta-519 cells, treated with STR, RTX-IgG1 or RTX-IgG3 or combinations thereof. Results shows mean ± SEM of three independent experiments, each with three biological replicates. Statistical analysis by one-way ANOVA with Tukey-Kramer post-hoc test (****p<0.0001). **(B)** Representative bivariate plots showing phagocytosis of CFSE-labeled Granta-519 target cells, treated with RTX isotypes alone or in combination with STR. Phagocytosis was quantified as the percentage of double positive CFSE$^+$ CTFR$^+$ MonoMac-6 cells (square gate). Increased phagocytosis was observed when RTX-IgG1 or RTX-IgG3 is combined with STR.

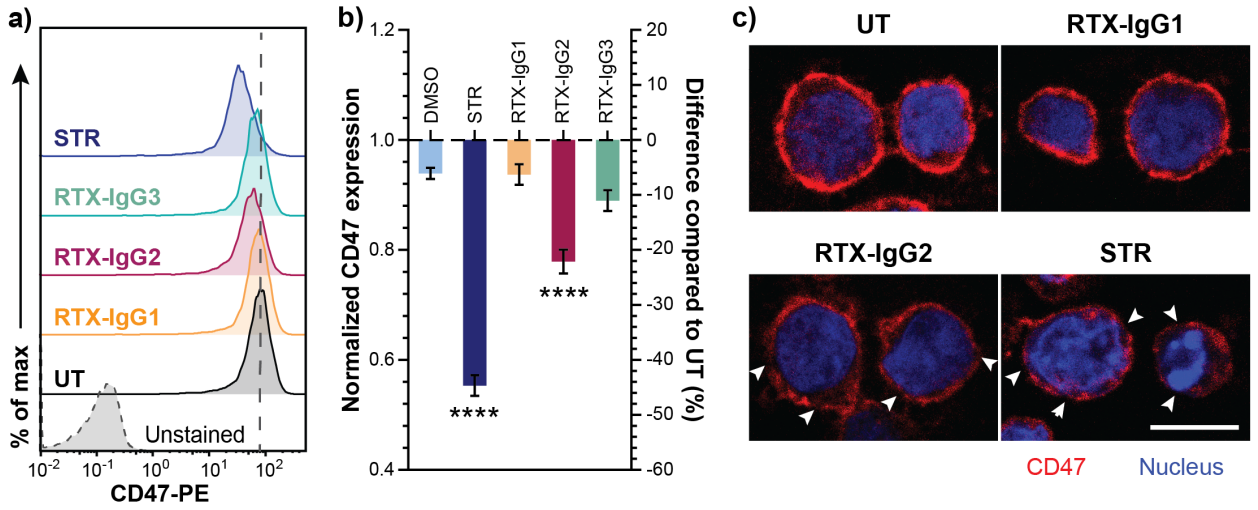

FIGURE 4
Decreased CD47 expression in RTX-IgG2-treated CD20$^+$ B-cell lymphoma cells. CD47 expression was evaluated in Granta-519 cells after incubation with STR (6 hours) or treatment with RTX isotypes (1.5 µg/mL) (30 min). **(A)** Representative histograms of CD47 expression in Granta-519 cells after treatment with RTX-IgG1, RTX-IgG2, RTX-IgG3, or STR. Grey dashed line indicates the level of CD47 on untreated cells (UT). **(B)** Bar graph representation of fold change (left Y-axis) and percentage difference (right Y-axis) in CD47 expression on Granta-519 cells induced by STR or RTX isotypes, normalized to CD47 expression on UT. To obtain the fold change values, mean fluorescence intensity (MFI) of treated samples was first adjusted by subtracting MFI of isotype controls and then normalized to the MFI of UT samples. The percentage difference was calculated by the following formula: $((MFI_{treated\ sample} - MFI_{UT})*100)/MFI_{UT}$). Results show mean fold change ± SEM of three independent experiments, each with three biological replicates. Statistical analysis by one-way ANOVA with Tukey-Kramer post-hoc test (****p<0.0001). **(C)** Confocal microscopy images of CD47 expression in untreated, RTX-IgG1-, RTX-IgG2-, and STR-treated Granta-519 cells. Cells were counterstained with Hoescht 33342 nucleus stain. Disruptions in CD47 cell surface pattern are indicated by white arrows. Scale bar: 10 µm.

CD47 expression, with CD47 redistributed into scattered clusters on the cell membrane (Figure 4C, lower panel). Remarkably, while STR and RTX-IgG2 induced similar levels of apoptosis, STR-treated cells exhibited signs of a later stage of apoptosis, such as nuclear deformation and condensed chromatin (visualized by Hoechst 33342 dye), which were absent in RTX-IgG2-treated cells (Figure 4C, lower panel).

3.5 RTX-IgG2 enhances the efficacy of other tumor-targeting mAbs in inducing ADCP of B-cell lymphoma cells

Since RTX-IgG2 was capable of altering and reducing the expression of CD47 on the target Granta-519 cells (Figure 4), we hypothesized that a pre-treatment of Granta-519 cells with RTX-IgG2 would enhance the efficacy of other tumor-targeting mAbs to induce ADCP. For this experiment, we chose two target molecules with different expression levels on Granta-519 cells – the immune checkpoint PD-L1 and the complement inhibitor CD59. As shown by Figure 5A, Granta-519 cells expressed the CD59 antigen markedly, while PD-L1 was weakly expressed (Figure 5B). When Granta-519 cells were treated with RTX-IgG2 in combination with mAbs targeting CD59 (αCD59) or PD-L1 (αPD-L1) antigens, the level of phagocytosis increased significantly compared to cells treated with αCD59 or αPD-L1 mAb alone (Figures 5C, D). Notably, the mAb targeting the highly expressed CD59 antigen mediated significant phagocytosis alone, in contrast to the mAb reactive to the low-expressing PD-L1 molecule. Correspondingly, RTX-IgG2 enhanced the phagocytic efficacy of αCD59 by 44% and of αPD-L1 by 31% (Table 1).

3.6 Blocking of CD47 enhances RTX-mediated phagocytosis

Our data suggested that the decreased levels of CD47 on the surface of Granta-519 cells, induced by RTX-IgG2 or STR, were associated with an enhancing effect on phagocytic activity by the MonoMac-6 effector cells. Therefore, in the next experiment, we used CD47-blocking mAbs, either with a functional or a silenced Fc domain, together with RTX-IgG1 or RTX-IgG3. As shown in Figure 6, blocking CD47 on the Granta-519 target cells significantly enhanced the phagocytic activity by MonoMac-6 cells. When combined with RTX-IgG1 and RTX-IgG3, the CD47-blocking Ab with a functional Fc domain (αCD47-fuFc) increased ADCP by 52% and 28%, respectively (Table 1). Meanwhile, the CD47-blocking Ab with a silenced Fc domain (αCD47-siFc) showed a modestly lower yet comparable enhancing effect on phagocytosis compared to the αCD47-fuFc, achieving an increase of 42% and 17% when combined with RTX-IgG1 and RTX-IgG3, respectively (Table 1). Notably, αCD47-fuFc alone triggered significant ADCP compared to untreated co-cultures, though at much lower level than when combined with RTX-IgG1 or RTX-IgG3 (Figure 6). The phagocytosis level induced by αCD47-fuFc (20% ± 3) was double that induced by αCD47-siFc alone (10% ± 1), underscoring the FcR-mediated phagocytosis induced by the Fc domain of the αCD47-fuFc.

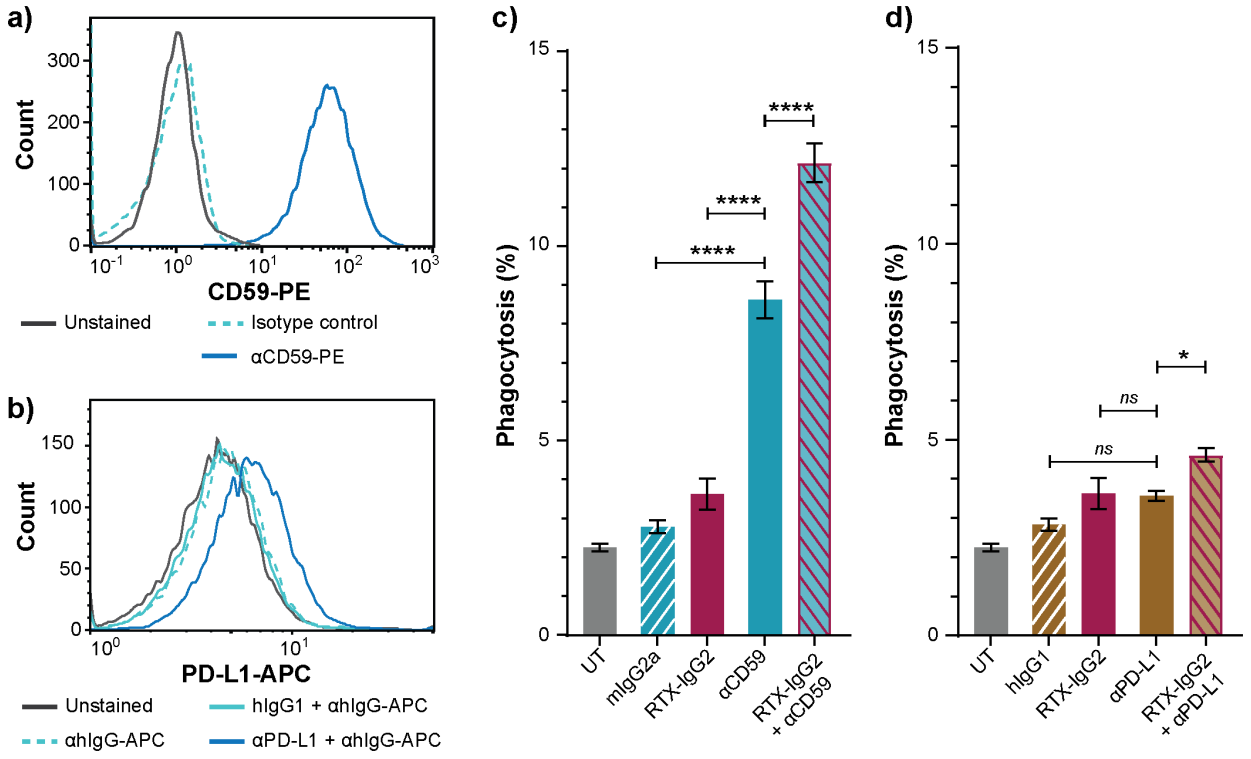

FIGURE 5
RTX-IgG2 enhances phagocytosis of CD20$^+$ B-cell lymphoma cells induced by anti-CD59 or anti-PD-L1 mAb. Representative histograms of **(A)** CD59 and **(B)** PD-L1 expression on Granta-519 cells. **(C, D)** Percentage phagocytosis of Granta-519 cells by MonoMac-6 cells (E:T ratio = 1:1), induced by c) mouse anti-human CD59 mAb (αCD59, 2.5 µg/mL) and d) human anti-PD-L1 mAb (αPD-L1, 1.5 µg/mL) alone, or in combination with a pre-treatment with RTX-IgG2. Data are presented as mean ± SEM of three independent experiments, each with three biological replicates. Statistical analysis by one-way ANOVA with Tukey-Kramer post-hoc test (****p<0.0001, *p<0.05; ns, not significant).

3.7 Lower CD20 and CD47 expression on tumor target cells diminishes the phagocytic-enhancing effect of RTX-IgG2

The effect of RTX-IgG2 was further validated on Raji B-cell lymphoma cells, which express lower levels of CD20, CD47, and CD59 compared to Granta-519 cells (Figure 7A, Supplementary Figure S6A). Notably, Raji cells demonstrated greater resistance to apoptosis, necessitating higher concentrations of STR (30 µM) and RTX-IgG2 (2.5 µg/mL) to achieve comparable levels of apoptosis and CD47 reduction as observed in Granta-519 cells treated with 7.5 µM of STR and 1.5 µg/mL of RTX-IgG2 (Figures 7B, C) (Figure 2A). The phagocytosis-enhancing effect of RTX-IgG2 on Raji cells was not observed when a higher concentration of RTX-IgG2 (2.5µg/mL) was used together with RTX-IgG1 or RTX-IgG3 (Figure 7D). However, when RTX-IgG2 was combined with a mAb targeting a non-CD20 molecule, such as CD59, enhanced phagocytosis of Raji cells was observed compared with anti-CD59 mAb alone (Figure 7E).

4 Discussion

Macrophages are the most abundant tumor-infiltrating immune cells in most human solid tumors, making them appealing therapeutic targets for cancer therapy (25, 26). However, their role as effector cells in cancer therapy remains underappreciated due to their intricate and polarized roles within the tumor microenvironment. A number of studies have associated a high content of tumor-infiltrating macrophages with unfavorable prognoses, especially in patients treated with certain chemotherapeutic agents (27–29). Conversely, macrophages have been shown to contribute significantly to the efficacy of mAb-based cancer immunotherapies through ADCP (8, 9, 30–33). In fact, macrophage infiltration has been shown to improve therapeutic responses in patients receiving a combined regimen of tumor-targeting mAb and chemotherapy (34). Additionally, monocytes – which express activating FcRs such as FcγRI (CD64) and FcγRIIa (CD32a) – have demonstrated the ability to eliminate tumor cells through ADCP as well (9–11). These lines of research necessitate further investigation on monocytes/macrophages-based cancer therapies to unlock their full anti-tumor potential.

Phagocytosis by macrophages/monocytes is mainly governed by the ubiquitously expressed “don’t-eat-me” CD47. Overexpression of CD47 has been shown to be associated with adverse prognosis in mantle cell lymphoma patients and play an important role in the dissemination of B-cell NHL (13) (35). Strategies targeting the interaction between CD47 and its receptor SIRP-α have demonstrated promising results either as monotherapies or in combination with other tumor-targeting therapies (36). However,

10.3389/fimmu.2024.1483617

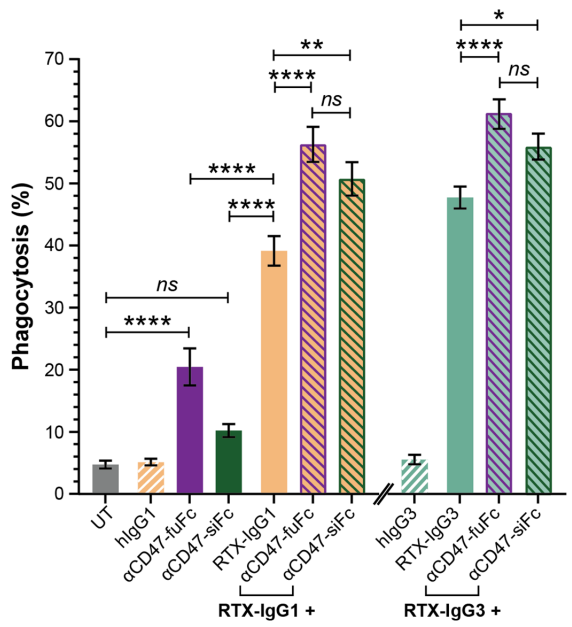

FIGURE 6
Blocking of CD47 on CD20$^+$ B-cell lymphoma cells enhances FcR-mediated ADCP. Percentage phagocytosis of Granta-519 cells treated with RTX-IgG1 or RTX-IgG3, and in combination with blocking of CD47 by mouse anti-human CD47 mAb with a functional Fc domain (αCD47-fuFc, 1 µg/mL) or humanized anti-CD47 mAb with a silenced Fc domain (αCD47-siFc, 10 µg/mL), by MonoMac-6 cells (E:T ratio = 2:1). Data are presented as mean ± SEM of three independent experiments, each with three biological replicates. Statistical analysis by one-way ANOVA with Tukey-Kramer post-hoc test (****p<0.0001, **p<0.01, *p <0.05; ns, not significant).

anti-CD47 therapies still encounter many setbacks in terms of selectivity, efficacy, and safety profile as CD47 is expressed not only on tumor cells but also on non-malignant cells.

In this study, utilizing the CD20$^+$CD47^{high} Granta-519 B-cell lymphoma cell line, we found that CD20-mediated apoptosis induced by RTX-IgG2 resulted in a reduction of CD47 expression on the Granta-519 cells. We also demonstrate that RTX-IgG2-treated lymphoma cells became significantly more susceptible to RTX-IgG1- or RTX-IgG3-mediated phagocytosis, which is consistent with our previous results (9). The apoptosis-inducer STR generated comparable levels of apoptosis as RTX-IgG2 and, similarly to RTX-IgG2, caused a reduction in CD47 expression, confirming the cause-effect relationship between apoptosis and CD47 reduction. STR also exhibited equivalent enhancing effect on phagocytosis when combined with RTX-IgG1 or RTX-IgG3. In support of our data, similar apoptosis associated decreased CD47 expression was reported by Gardai et al. (17). It is important to note that STR-induced effects are unselective and independent of CD20, resulting in high levels of background apoptosis. In contrast, RTX-IgG2 specifically targets only CD20$^+$ cells.

While apoptosis induction by RTX-IgG2 has been previously reported, its exact mechanism remains incompletely understood (9, 37). Compared to RTX-IgG1, RTX-IgG2 induces similar level of homotypic adhesion (Supplementary Figure S4), while exhibiting a substantially reduced ability to induce ADCP and CDC (6, 9, 37). In fact, RTX-IgG2 binds CD20$^+$ B-cell lymphoma cells at only half the density of RTX-IgG1 and RTX-IgG3 (Supplementary Figure S7) (37), but induces significantly more apoptosis in these cells (9, 37). For these reasons, we propose that RTX-IgG2, although binding to the same CD20 epitope as RTX-IgG1, attaches in different binding modes and geometries, in support of the hypothesis by Konitzer et al. (37). Among all IgG isotypes, IgG2 possesses the most rigid hinge region and unique alternative covalent links between its Fab domains and the hinge (38, 39). Given the significant differences in the hinge region of IgG2, it is reasonable to speculate that these distinct structural features may affect its binding geometry to target receptor (37, 40–42). Indeed, recent studies have correlated the rigidity of the IgG2 hinge with agonistic function (40, 43, 44), suggesting that mAbs of the IgG2 isotype can elicit agonistic activity upon target binding by closely crosslinking target receptors, thereby promoting downstream signaling (40–45). Based on these literature, here, we attribute the apoptosis-inducing ability of RTX-IgG2 to its unique hinge structure and the resulted agonistic activity.

To our knowledge, our experiment is the first that associates RTX-IgG2-mediated apoptosis with a reduced CD47 expression and an enhancing effect on phagocytosis. We also reveal with microscopic analysis that the pattern of CD47 expression on the surface of RTX-IgG2-treated cells shifts from a homogeneous distribution to a more clustered arrangement. A similar change in spatial distribution of CD47 has previously been reported in aged mouse erythrocytes and human Jurkat T-cells (17, 20). These studies, together with our observation, suggest that apoptosis trigger major structural alterations of the cell plasma membrane, which may either destabilize lateral molecular interactions needed for the proper CD47 "don't-eat-me" signaling (17, 20) or induce conformation changes of CD47, hindering its interaction with SIRP-α (46).

Based on these findings, we hypothesized that pre-treatment with the agonistic RTX-IgG2 – which reduces the anti-phagocytic CD47 on the surface of target cells – could enhance the phagocytic efficacy of other tumor-targeting mAbs. Indeed, RTX-IgG2 pre-treatment significantly increased the phagocytosis of Granta-519 cells when combined with anti-CD59 or anti-PD-L1 mAbs. Importantly, a higher expression level of the target molecules correlated with a higher level of enhanced phagocytosis, as demonstrated by CD59. Notably, targeting of low-expressing tumor antigens, such as PD-L1 on Granta-519 cells, can still be enhanced by RTX-IgG2. The efficacy of RTX-IgG2 as a phagocytic enhancer improves when it does not need to compete with mAbs targeting the same antigen/epitope (CD20). Indeed, similar CD47-reducing and phagocytosis-enhancing effects by RTX-IgG2 were also evident in CD47^{low} Raji cells when RTX-IgG2 was combined with anti-CD59 mAbs, but not with RTX-IgG1 or RTX-IgG3.

Collectively, our results highlight the role of RTX-IgG2 as an exclusive and target-specific enhancer for FcR-mediated phagocytosis of CD20$^+$ B-cell lymphoma cells, an effect associated with induction of apoptosis and reduction of CD47 on target cells.

Considering that the downregulation of CD47 is essential in driving the ADCP enhancement by RTX-IgG2, we conducted a

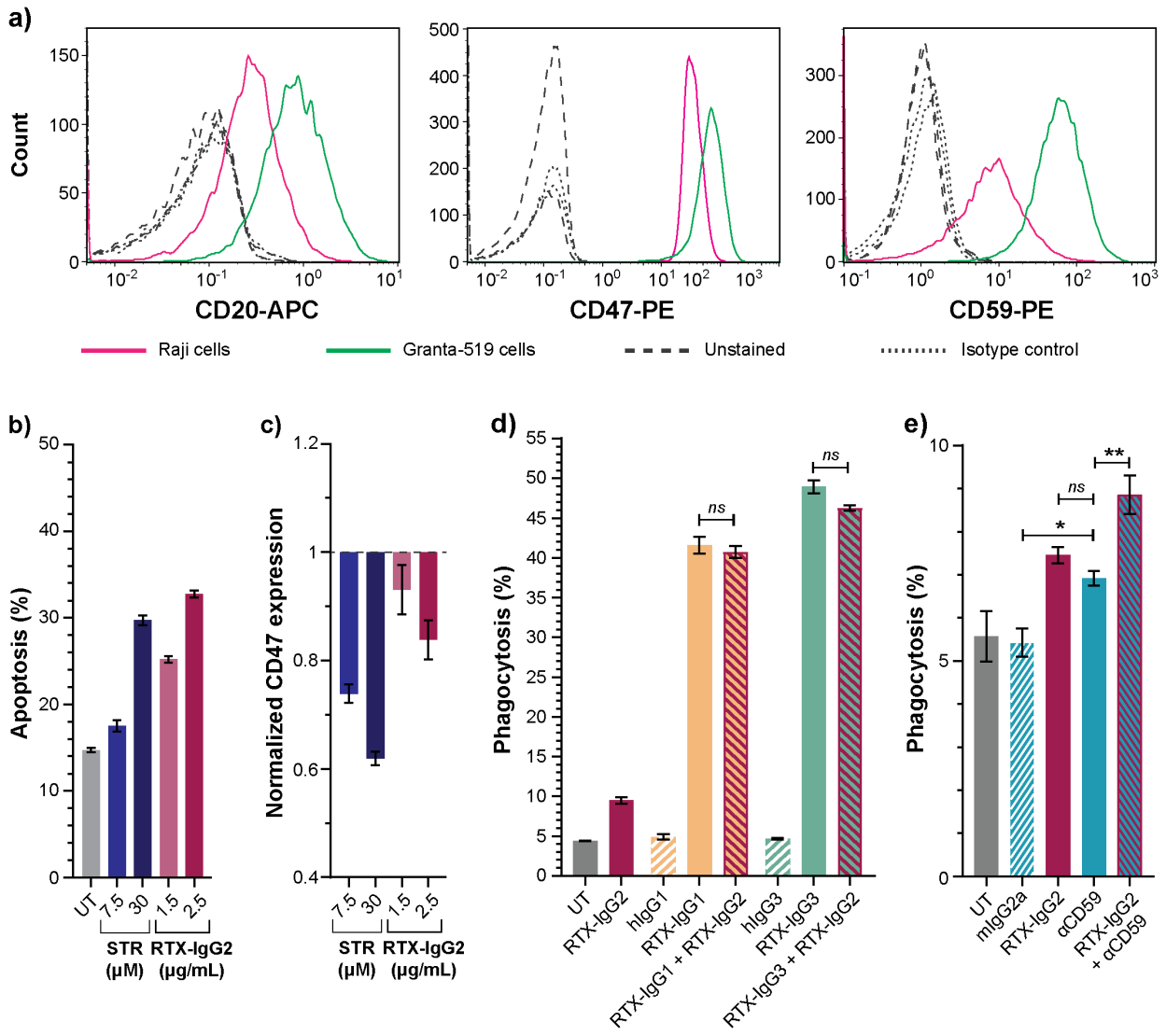

FIGURE 7
Effects of RTX-IgG2 on Raji B-cell lymphoma cells. **(A)** Representative histograms of CD20, CD47, and CD59 expression on Raji and Granta-519 B-cell lymphoma cells. **(B)** Percentage apoptosis in untreated (UT) and STR- or RTX-IgG2-treated Raji cells. **(C)** Fold change in CD47 expression on Raji cells induced by STR or RTX-IgG2, normalized to CD47 expression on untreated cells (UT). **(D)** Percentage phagocytosis of Raji cells by MonoMac-6 cells (E:T ratio = 1:1), induced by single RTX isotypes, or dual combinations of RTX-IgG2 with RTX-IgG1 or RTX-IgG3. Untreated cells (UT), and human Ab isotypes (hIgG1, hIgG2, hIgG3) were used as controls. For dual treatments, Raji cells were pre-opsonized with 2.5 μg/mL of RTX-IgG2 for 30 min followed by 1.5 μg/mL of RTX-IgG1 or RTX-IgG3. **(E)** Percentage phagocytosis of Raji cells by MonoMac-6 cells (E:T ratio = 1:1), induced by mouse anti-human CD59 mAb (αCD59, 2.5 μg/mL) alone, or in combination with a pre-treatment with RTX-IgG2. Results in **(B-E)** are shown as mean ± SEM of three biological replicates from one representative experiment out of two. Statistical analysis by one-way ANOVA with Tukey-Kramer post-hoc test (**p<0.01, *p<0.05; ns, not significant).

CD47-blocking experiment to further validate our findings. For this experiment, we used two different versions of CD47-blocking mAbs: a commercially available mouse IgG2a anti-human CD47 Ab (αCD47-fuFc) and an engineered humanized IgG2 anti-CD47 Ab harboring a completely silenced Fc domain (αCD47-siFc) (23). Both CD47-blocking mAbs effectively enhanced the phagocytic uptake of Granta-519 cells by MonoMac-6 cells when combined with RTX-IgG1 or RTX-IgG3 (Table 1). However, αCD47-fuFc alone exerted notable Fc-mediated phagocytosis, suggesting potential on-target, off-tumor effects. The pronounced phagocytosis induced by αCD47-fuFc was likely mediated by its functional Fc domain, complicating the assessment of whether a synergistic effect between this Ab and RTX-IgG1 and RTX-IgG3 was achieved. In contrast, the αCD47-siFc alone induced negligible phagocytosis, indicating effective abrogation of undesired Fc-mediated engagement. This experiment conclusively confirmed that blocking CD47 can synergistically enhance RTX-mediated phagocytosis, provided that the CD47-blocking mAb is carefully designed to avoid undesired Fc receptor engagement on effectors cells and consequent toxicity. As agonistic activity of IgG2 mAbs

has been demonstrated to occur independently of FcγR engagement (41), further utilization of αCD47-siFc warrants comprehensive analyses of its potential agonistic effects.

In conclusion, our *in vitro* studies show that RTX-IgG2, in combination with tumor-targeting mAbs, enhances ADCP of $CD20^+$ B-cell lymphoma cells via CD20-mediated apoptosis and CD47 reduction. This suggests that RTX-IgG2 could serve as a valuable agonist for B-cell NHL therapy and additionally be used to improve efficacy of RTX treatment of other B-cell disorders. Developing tumor-specific IgG2 mAbs with apoptotic capacity presents a promising approach to enhance antibody-based immunotherapy. To improve clinical relevance, future studies should incorporate three-dimensional human B-cell lymphoma models or xenograft mouse models to better assess therapeutic efficacy.

Data availability statement

The raw data supporting the conclusions of this article will be made available by the authors, without undue reservation.

Ethics statement

Ethical approval was not required for the studies on humans in accordance with the local legislation and institutional requirements because only commercially available established cell lines were used.

Author contributions

ON: Writing – original draft, Writing – review & editing, Data curation, Formal analysis, Investigation, Methodology, Validation, Visualization. SL: Writing – review & editing. GF: Writing – review & editing. MP: Writing – review & editing. SK: Conceptualization, Funding acquisition, Methodology, Project administration, Resources, Supervision, Writing – review & editing.

Funding

The author(s) declare financial support was received for the research, authorship, and/or publication of this article. This work was financially supported by Uppsala University.

Acknowledgments

The authors thank the staff at the BioVis facility, especially Jeremy Adler (Rudbeck Laboratory, Uppsala University, Uppsala, Sweden), and Inkyung Jang (Department of Cell and Molecular Biology, Uppsala University) for technical support.

Conflict of interest

The authors declare that the research was conducted in the absence of any commercial or financial relationships that could be construed as a potential conflict of interest.

Publisher's note

Supplementary material

The Supplementary Material for this article can be found online at: https://www.frontiersin.org/articles/10.3389/fimmu.2024.1483617/full#supplementary-material

References

1. Sun HF, Xue L, Guo YH, Du JQ, Nan KJ, Li M. Global, regional and national burden of non-Hodgkin lymphoma from 1990 to 2017: estimates from global burden of disease study in 2017. *Ann Med.* (2022) 54:633–45. doi: 10.1080/07853890.2022.2039957

2. O'Connor OA, Tobinai K. Putting the clinical and biological heterogeneity of non-Hodgkin lymphoma into context. *Clin Cancer Res.* (2014) 20:5173–81. doi: 10.1158/1078-0432.Ccr-14-0574

3. Smith MR. Rituximab (monoclonal anti-CD20 antibody): mechanisms of action and resistance. *Oncogene.* (2003) 22:7359–68. doi: 10.1038/sj.onc.1206939

4. Pierpont TM, Limper CB, Richards KL. Past, present, and future of rituximab - the world's first oncology monoclonal antibody therapy. *Front Oncol.* (2018) 8:163. doi: 10.3389/fonc.2018.00163

5. Johnson P, Glennie M. The mechanisms of action of rituximab in the elimination of tumor cells. *Semin Oncol.* (2003) 30:3–8. doi: 10.1053/sonc.2003.50025

6. Glennie MJ, French RR, Cragg MS, Taylor RP. Mechanisms of killing by anti-CD20 monoclonal antibodies. *Mol Immunol.* (2007) 44:3823–37. doi: 10.1016/j.molimm.2007.06.151

7. Boross P, Leusen JHW. Mechanisms of action of CD20 antibodies. *Am J Cancer Res.* (2012) 2:676–90.

8. Lefebvre ML, Krause SW, Salcedo M, Nardin A. Ex vivo-activated human macrophages kill chronic lymphocytic leukemia cells in the presence of rituximab: mechanism of antibody-dependent cellular cytotoxicity and impact of human serum. *J Immunother.* (2006) 29:388–97. doi: 10.1097/01.cji.0000203081.43235.d7

9. Lara S, Anania JC, Virtanen A, Stenhammar V, Kleinau S. Importance of antibody isotypes in antitumor immunity by monocytes and complement using human-immune tumor models. *Eur J Immunol.* (2021) 51:1218–33. doi: 10.1002/eji.202048885

10. Kleinau S. Impact of Fc receptors and host characteristics on myeloid phagocytic response to rituximab-treated 3D-cultured B-cell lymphoma. *Immunother Adv.* (2023) 3. doi: 10.1093/immadv/ltad025

11. Uchida JJ, Hamaguchi Y, Oliver JA, Ravetch JV, Poe JC, Haas KM, et al. The innate mononuclear phagocyte network depletes B lymphocytes through Fc receptor-dependent mechanisms during anti-CD20 antibody immunotherapy. *J Exp Med.* (2004) 199:1659–69. doi: 10.1084/jem.20040119

12. Minard-Colin V, Xiu Y, Poe JC, Horikawa M, Magro CM, Hamaguchi Y, et al. Lymphoma depletion during CD20 immunotherapy in mice is mediated by macrophage FcγRI, FcγRIII, and FcγRIV. *Blood.* (2008) 112:1205–13. doi: 10.1182/blood-2008-01-135160

13. Chao MP, Alizadeh AA, Tang C, Myklebust JH, Varghese B, Gill S, et al. Anti-CD47 antibody synergizes with rituximab to promote phagocytosis and eradicate non-Hodgkin lymphoma. *Cell*. (2010) 142:699–713. doi: 10.1016/j.cell.2010.07.044

14. Brown EJ, Frazier WA. Integrin-associated protein (CD47) and its ligands. *Trends Cell Biol*. (2001) 11:130–5. doi: 10.1016/S0962-8924(00)01906-1

15. Bouwstra R, van Meerten T, Bremer E. CD47-SIRPα blocking-based immunotherapy: Current and prospective therapeutic strategies. *Clin Transl Med*. (2022) 12:e943. doi: 10.1002/ctm2.943

16. Russ A, Hua AB, Montfort WR, Rahman B, Bin Riaz I, Khalid MU, et al. Blocking "don't eat me" signal of CD47-SIRPα in hematological Malignancies, an in-depth review. *Blood Rev*. (2018) 32:480–9. doi: 10.1016/j.blre.2018.04.005

17. Gardai SJ, McPhillips KA, Frasch SC, Janssen WJ, Starefeldt A, Murphy-Ullrich JE, et al. Cell-surface calreticulin initiates clearance of viable or apoptotic cells through trans-activation of LRP on the phagocyte. *Cell*. (2005) 123:321–34. doi: 10.1016/j.cell.2005.08.032

18. Lv Z, Bian Z, Shi L, Niu S, Ha B, Tremblay A, et al. Loss of cell surface CD47 clustering formation and binding avidity to SIRPα Facilitate apoptotic cell clearance by macrophages. *J Immunol*. (2015) 195:661–71. doi: 10.4049/jimmunol.1401719

19. Burger P, Hilarius-Stokman P, de Korte D, van den Berg TK, van Bruggen R. CD47 functions as a molecular switch for erythrocyte phagocytosis. *Blood*. (2012) 119:5512–21. doi: 10.1182/blood-2011-10-386805

20. Wang F, Liu YH, Zhang T, Gao J, Xu Y, Xie GY, et al. Aging-associated changes in CD47 arrangement and interaction with thrombospondin-1 on red blood cells visualized by super-resolution imaging. *Aging Cell*. (2020) 19:e13224. doi: 10.1111/acel.13224

21. Métayer LE, Vilalta A, Burke GAA, Brown GC. Anti-CD47 antibodies induce phagocytosis of live, Malignant B cells by macrophages via the Fc domain, resulting in cell death by phagoptosis. *Oncotarget*. (2017) 8:60892–903. doi: 10.18632/oncotarget.18492

22. Abrisqueta P, Sancho JM, Cordoba R, Persky DO, Andreadis C, Huntington SF, et al. Anti-CD47 antibody, CC-90002, in combination with rituximab in subjects with relapsed and/or refractory non-Hodgkin lymphoma (R/R NHL). *Blood*. (2019) 134 (Supplement_1):4089. doi: 10.1182/blood-2019-125310

23. Zeller T, Lutz S, Münnich IA, Windisch R, Hilger P, Herold T, et al. Dual checkpoint blockade of CD47 and LILRB1 enhances CD20 antibody-dependent phagocytosis of lymphoma cells by macrophages. *Front Immunol*. (2022) 13:929339. doi: 10.3389/fimmu.2022.929339

24. Schneider D, Xiong Y, Wu D, Nölle V, Schmitz S, Haso W, et al. A tandem CD19/CD20 CAR lentiviral vector drives on-target and off-target antigen modulation in leukemia cell lines. *J Immunother Cancer*. (2017) 5:42. doi: 10.1186/s40425-017-0246-1

25. Liu Y, Wang YJ, Yang YR, Weng LJ, Wu Q, Zhang J, et al. Emerging phagocytosis checkpoints in cancer immunotherapy. *Signal Transduct Tar*. (2023) 8:104. doi: 10.1038/s41392-023-01365-z

26. Gentles AJ, Newman AM, Liu CL, Bratman SV, Feng WG, Kim D, et al. The prognostic landscape of genes and infiltrating immune cells across human cancers. *Nat Med*. (2015) 21:938–45. doi: 10.1038/nm.3909

27. Farinha P, Masoudi H, Skinnider BF, Shumansky K, Spinelli JJ, Gill K, et al. Analysis of multiple biomarkers, shows that lymphoma-associated macrophage (LAM) content is an independent predictor of survival in follicular lymphoma (FL). *Blood*. (2005) 106:2169–74. doi: 10.1182/blood-2005-04-1565

28. Steidl C, Lee T, Shah SP, Farinha P, Han G, Nayar T, et al. Tumor-associated macrophages and survival in classic Hodgkin's lymphoma. *New Engl J Med*. (2010) 362:875–85. doi: 10.1056/NEJMoa0905680

29. Mantovani A, Allavena P, Marchesi F, Garlanda C. Macrophages as tools and targets in cancer therapy. *Nat Rev Drug Discovery*. (2022) 21:799–820. doi: 10.1038/s41573-022-00520-5

30. Oflazoglu E, Stone IJ, Gordon KA, Grewal IS, van Rooijen N, Law CL, et al. Macrophages contribute to the antitumor activity of the anti-CD30 antibody SGN-30. *Blood*. (2007) 110:4370–2. doi: 10.1182/blood-2007-06-097014

31. Oflazoglu E, Stone IJ, Brown L, Gordon KA, van Rooijen N, Jonas M, et al. Macrophages and Fc-receptor interactions contribute to the antitumour activities of the anti-CD40 antibody SGN-40. *Brit J Cancer*. (2009) 100:113–7. doi: 10.1038/sj.bjc.6604812

32. Watanabe M, Wallace PK, Keler T, Deo YM, Akewanlop C, Hayes DF. Antibody dependent cellular phagocytosis (ADCP) and antibody dependent cellular cytotoxicity (ADCC) of breast cancer cells mediated by bispecific antibody, MDX-210. *Breast Cancer Res Tr*. (1999) 53:199–207. doi: 10.1023/A:1006145507567

33. Weiskopf K, Weissman IL. Macrophages are critical effectors of antibody therapies for cancer. *MAbs*. (2015) 7:303–10. doi: 10.1080/19420862.2015.1011450

34. Taskinen M, Karjalainen-Lindsberg ML, Nyman H, Eerola LM, Leppä S. A high tumor-associated macrophage content predicts favorable outcome in follicular lymphoma patients treated with rituximab and cyclophosphamide-doxorubicin-vincristine-prednisone. *Clin Cancer Res*. (2007) 13:5784–9. doi: 10.1158/1078-0432.Ccr-07-0778

35. Chao MP, Tang C, Pachynski RK, Chin R, Majeti R, Weissman IL. Extranodal dissemination of non-Hodgkin lymphoma requires CD47 and is inhibited by anti-CD47 antibody therapy. *Blood*. (2011) 118:4890–901. doi: 10.1182/blood-2011-02-338020

36. Eladl E, Tremblay-LeMay R, Rastgoo N, Musani R, Chen WM, Liu AJ, et al. Role of CD47 in hematological Malignancies. *J Hematol Oncol*. (2020) 13:96. doi: 10.1186/s13045-020-00930-1

37. Konitzer JD, Sieron A, Wacker A, Enenkel B. Reformatting rituximab into human IgG2 and IgG4 isotypes dramatically improves apoptosis induction *in vitro*. *PloS One*. (2015) 10. doi: 10.1371/journal.pone.0145633

38. Roux KH, Strelets L, Michaelsen TE. Flexibility of human IgG subclasses. *J Immunol*. (1997) 159:3372–82. doi: 10.4049/jimmunol.159.7.3372

39. Wypych J, Li M, Guo A, Zhang ZQ, Martinez T, Allen MJ, et al. Human IgG2 antibodies display disulfide-mediated structural isoforms. *J Biol Chem*. (2008) 283:16194–205. doi: 10.1074/jbc.M709987200

40. Yu XJ, Chan HTC, Fisher H, Penfold CA, Kim J, Inzhelevskaya T, et al. Isotype switching converts anti-CD40 antagonism to agonism to elicit potent antitumor activity. *Cancer Cell*. (2020) 37:850–66. doi: 10.1016/j.ccell.2020.04.013

41. White AL, Chan HTC, French RR, Willoughby J, Mockridge CI, Roghanian A, et al. Conformation of the human immunoglobulin G2 hinge imparts superagonistic properties to immunostimulatory anticancer antibodies. *Cancer Cell*. (2015) 27:138–48. doi: 10.1016/j.ccell.2014.11.001

42. Orr CM, Fisher H, Yu XJ, Chan CHT, Gao YY, Duriez PJ, et al. Hinge disulfides in human IgG2 CD40 antibodies modulate receptor signaling by regulation of conformation and flexibility. *Sci Immunol*. (2022) 7:eabm3723. doi: 10.1126/sciimmunol.abm3723

43. Liu XB, Zhao YJ, Shi H, Zhang Y, Yin XY, Liu MD, et al. Human immunoglobulin G hinge regulates agonistic anti-CD40 immunostimulatory and antitumour activities through biophysical flexibility. *Nat Commun*. (2019) 10:10. doi: 10.1038/s41467-019-12097-6

44. Allen MJ, Guo A, Martinez T, Han M, Flynn GC, Wypych J, et al. Interchain disulfide bonding in human IgG2 antibodies probed by site-directed mutagenesis. *Biochemistry-Us*. (2009) 48:3755–66. doi: 10.1021/bi8022174

45. Yu XJ, James S, Felce JH, Kellermayer B, Johnston DA, Chan HTC, et al. TNF receptor agonists induce distinct receptor clusters to mediate differential agonistic activity. *Commun Biol*. (2021) 4:772. doi: 10.1038/s42003-021-02309-5

46. Dufour S, Tacnet-Delorme P, Kleman JP, Glushonkov O, Thielens N, Bourgeois D, et al. Nanoscale imaging of CD47 informs how plasma membrane modifications shape apoptotic cell recognition. *Commun Biol*. (2023) 6:207. doi: 10.1038/s42003-023-04558-y